Journal of Thermal Analysis and Calorimetry (2021) 145:361–378
https://doi.org/10.1007/s10973-020-09753-1

Pharmaceutical compatibility of dexamethasone with excipients commonly used in solid oral dosage forms

Widson M. Santos[1] · Fernanda P. Nóbrega[1] · Jéssica C. Andrade[1] · Lucas F. Almeida[1] · Marta M. Conceição[2] · Ana Cláudia D. Medeiros[1] · Francinalva D. Medeiros[1,3]

Received: 17 February 2019 / Accepted: 27 April 2020 / Published online: 12 May 2020

Abstract
Dexamethasone is a glucocorticoid drug used for the treatment of acute and chronic inflammatory conditions, autoimmune diseases, some cancers, and several other pathologies. It is widely marketed worldwide especially under solid dosage forms. This study aimed to assess its compatibility with solid pharmaceutical excipients. Compatibility study was conducted through the preparation of binary mixtures (1:1, w/w) of dexamethasone with 12 selected excipients. Binary mixtures were analyzed by thermoanalytical techniques (thermogravimetric and differential thermal analysis), Fourier transform infrared spectroscopy, and X-ray diffraction. TG curves pointed only slight anticipations of dexamethasone decomposition. DTA curves showed interactions signs with microcrystalline cellulose 101 and 102, magnesium stearate, mannitol, and polyvinylpyrrolidone. Drug infrared absorption profile was not affected by the mixture with most excipients. X-ray diffractograms of all binary mixtures did not exhibit signs of interactions with changes of dexamethasone crystalline state. These results pointed that the interactions found by DTA technique were probably heat-induced. Therefore, the above-mentioned excipients should be carefully used in solid dosage forms with heat-based manufacturing processes.

Keywords API–excipient compatibility · Glucocorticoids · Thermal analysis · TG · DTA · Preformulation studies

Introduction

Preformulation studies involve a series of investigations aimed to the rational formulation of an active pharmaceutical ingredient (API). In these studies, physicochemical and biopharmaceutical characteristics of APIs and excipients are rigorously evaluated individually and/or in combination [1]. The International Conference on Harmonization of Technical Requirements for Registration of Pharmaceuticals for Human Use (ICH), through the guideline Q8 (R2), establishes that these studies are important for the development of quality pharmaceuticals and define the best manufacturing process to ensure the intended product performance [2]. Preformulation studies should be conducted during the development of new drugs or in generic products formulation [3].

Pharmaceutical excipients are defined as any component other than the API added to a drug formulation. They have several functional properties in a pharmaceutical product, including manufacturing process improvement, API vehicle and protection, administration enablement, improvement of stability, bioavailability and patient acceptability, besides ensuring drug release and efficacy during storage and use [4]. Most excipients do not have direct pharmacological activity, but its irrational use may seriously affect the drug properties. API–excipients interactions may occur during drug manufacturing and/or storage, resulting in changes of physical, chemical and therapeutic properties of the drug [5, 6].

API–excipient interactions are classified into two types: physical or chemical. In physical interactions, there are no chemical bonds or changes of drug molecular structure, but

✉ Ana Cláudia D. Medeiros
anaclaudia@uepb.edu.br

[1] Laboratório de Desenvolvimento e Ensaios de Medicamentos, Centro de Ciências Biológicas e da Saúde, Universidade Estadual da Paraíba, 351, Cidade Universitária, 58429-500 Campina Grande, PB, Brazil

[2] Centro de Tecnologia e Desenvolvimento Regional, Universidade Federal da Paraíba, João Pessoa, PB 58058-600, Brazil

[3] Centro de Educação e Saúde, Universidade Federal de Campina Grande, Sítio Olho D'água da Bica, S/N, Cidade Universitária, Cuité, PB 58175-000, Brazil

there are modifications of some physicochemical properties such as solubility and dissolution rate, which can affect drug bioavailability. Physical interactions may also affect organoleptic properties (color, odor and taste), drug release, solid state, polymorphic form, tensile strength, among others. Chemical interactions can induce drug degradation and formation of degradation products, which can be toxic and result in potency loss [7, 8]. In this scenario, several researches focused on the development of new medicines (of synthetic or natural origin) have conducted compatibility studies for proper excipient selection [9–13]. At the same time, some studies have reported API–excipients incompatibilities of drugs already on the market [5, 14–17].

API–excipient compatibility studies are an important stage of preformulation studies. They are conducted to rigorously investigate physical and chemical interactions and ensure the rational formulation of the drug. The thermoanalytical techniques, including thermogravimetry (TG) and differential thermal analysis (DTA), are widely used for rapid and preliminary assessment of interactions. DTA technique is an efficient tool to predict interactions by comparing the curves of the individual components (APIs and excipients) with the curve of their respective physical mixture. Indications of interactions are verified through appearance, disappearance, shifting and/or enthalpy variations of endothermic/exothermic peaks in the physical mixtures curves. TG is a useful technique to assess the influence of excipients on the thermal stability of the API [18–20].

However, thermoanalytical results should be carefully analyzed to avoid erroneous conclusions. These techniques expose samples to very high temperatures that do not occur during drug manufacturing or storage, and consequently, interactions can be induced through heating. Furthermore, the use of complementary techniques such as Fourier transform infrared (FTIR) and X-ray diffraction (XRD) is indispensable [21]. FTIR technique is used to investigate intermolecular interactions and other that result in desalination, hydrate formation, dehydration, polymorphic changes, and transition from crystalline to amorphous state or vice versa [22]. XRD technique is widely used to search for interactions that affect API crystallinity, amorphity, or polymorphic form [7].

Dexamethasone (DEX) (9-fluoro-11β, 17,21-trihydroxy-16α-methylpregna-1,4-diene-3,20-dione ($C_{22}H_{29}FO_5$)) is a cyclopentaneperhydrophenanthrene nucleus derivative (Fig. 1) [23]. It is a glucocorticoid drug widely used for the treatment of chronic and acute inflammatory conditions, autoimmune diseases, some cancers, and several other pathologies. It acts on the glucocorticoid receptors (GR) and, through several complex mechanisms, modifies genetic transcription, increasing anti-inflammatory proteins, and decreasing pro-inflammatory proteins levels. Briefly, dexamethasone inhibits nuclear translocation and

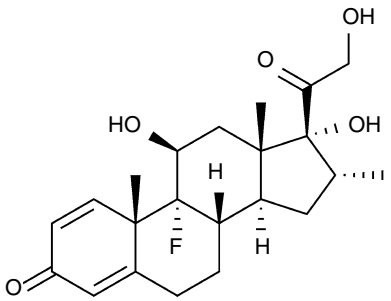

Fig. 1 Chemical structure of DEX

transcription factors functions of several proinflammatory proteins, including interleukin 1, interleukin 2, tumor necrosis factor α, interferon γ, and prostaglandins [24, 25].

DEX is widely marketed under several dosage forms, including oral tablets; ophthalmic, intramuscular, intravenous, intralesional, and intra-articular solutions; and oral elixirs [26]. To date, there is no information in the literature about its compatibility with pharmaceutical excipients. In addition, Brazilian medicines marketed before the inauguration of the Agência Nacional de Vigilância Sanitária (ANVISA) were not properly submitted to preformulation studies due to the inefficient health legislation in force at the time. In this context, our study aims to assess the pharmaceutical compatibility of dexamethasone with excipients commonly used in solid oral dosage forms.

Materials and methods

DEX was purchased from Valdequímica Produtos Químicos Ltda. (Caxingui, São Paulo, Brazil). Colloidal silicon dioxide, magnesium stearate, mannitol, mycrocristalline cellulose 102, pregelatinized starch, sodium starch glycolate, and polyvinylpirrolidone k-30 were purchased from Henrifarma Produtos Químicos e Farmacêutico Ltda. (Cambuci, São Paulo, Brazil). Mycrocristalline cellulose 101 and lactose monohydrate were purchased from Galena Química e Farmacêutica Ltda. (Campinas, São Paulo, Brazil). Talc was purchased from Sintética Distribuidora Química Farmacêutica Ltda. (Capivari, São Paulo, Brazil).

Physical mixtures

Binary mixtures (1:1, w w^{-1}) of DEX with each excipient were prepared by simple mixing using porcelain pestle and mortar. Posteriorly, mixtures were placed in polypropylene microtubes and stored at room temperature till further analysis. Functional categories of each selected excipient are described in Table 1. All the individual components and

Table 1 Abbreviations and functional categories of the solid pharmaceutical excipients used in the compatibility study

Excipients	Abbreviation	Functional category
Colloidal silicon dioxide	CSD	Disintegrant
Croscarmellose sodium	CCS	Disintegrant
Lactose monohydrate	LAC	Binder, diluent
Magnesium stearate	MS	Lubricant
Mannitol	MAN	Diluent
Microcrystalline cellulose 101	MC101	Diluent, disintegrant
Microcrystalline cellulose 102	MC102	Diluent, disintegrant
Polyvinylpyrrolidone k-30	PVP	Disintegrant
Pregelatinized starch	PgSTA	Diluent, disintegrant, binder
Sodium starch glycolate	SSG	Disintegrant
Starch	STA	Diluent, disintegrant, binder
Talc	TAL	Diluent, lubricant

their binary mixtures were analyzed by the analytical techniques described below.

Thermogravimetric analysis (TG)

The TG analyses were performed on a DTG-60 simultaneous TG/DTA thermal analyzer (Shimadzu, Kyoto, Japan). Approximately, 8 mg of samples was analyzed in open alumina crucibles, under dynamic nitrogen atmosphere (50 mL min^{-1}), heating rate of 10 °C min^{-1} and temperature range from 30 to 900 °C. Calcium oxalate monohydrate was used as standard for equipment calibration. The first derivative of TG curves (DTG) was used to identify the degradation steps of each sample.

Differential thermal analysis (DTA)

The DTA analyses were performed on a DTG-60 simultaneous TG/DTA thermal analyser (Shimadzu). Approximately, 2 mg of samples were analyzed in sealed aluminum crucibles, under dynamic nitrogen atmosphere (50 mL min^{-1}), heating rate of 10 °C min^{-1} and temperature range from 30 to 450 °C. Indium (melting point 156.6 °C) was used as standard for equipment calibration.

The Fourier Transformed Infrared Spectroscopy (FTIR)

FTIR spectra were recorded on an IR Prestige spectrophotometer (Shimadzu) in the range of 4000–600 cm^{-1} and resolution of 4 cm^{-1}.

X-ray powder diffraction (XRD)

The XRD patterns were recorded on a XRD 6000 diffractometer (Shimadzu) using radiation source of Cu Kα. The scanned range was 5°–45° (2θ) at a digitalization speed of 2° min^{-1}. The equipment was operated on a voltage of 40.0 kV and current of 30.0 mA.

Results and discussion

DEX thermal profile

The TG/DTG curves showed that DEX is stable, with no mass loss events, up to 256.60 °C. Three degradation steps were observed between 256.60 and 454.49 °C with mass loss (Δm) of 89% (Fig. 2a). DTA curve showed an endothermic peak characteristic of melting at 254.86 °C and an exothermic peak at 270.48 °C attributed to the decomposition process (Fig. 2b). The melting point detected for DEX is slightly below the value of 255.00 °C informed by the Brazilian and Japanese Pharmacopoeias [27, 28]. Combined analysis of TG/DTG and DTA curves showed that DEX decomposition starts immediately after its fusion. Similar thermal profile for DEX was reported by Oliveira et al. [29].

Thermal compatibility by TG

The TG/DTG parameters of each individual component (API or excipient) and their binary mixtures are shown in Table 2.

Croscarmellose sodium (CCS) first showed a surface water loss event at 38.27–79.22 °C, then a major decomposition event at 282.34–309.35 °C, followed by gradual mass loss with increasing temperature. This excipient showed high ash content (21.97%) due to its molecular sodium. In DEX + CCS mixture, decomposition was slightly anticipated (T_{onset} = 246.11 °C) when compared with each individual compound (Fig. 3a).

Colloidal silicon dioxide (CSD) did not exhibit mass loss events within the studied temperature range due to its inorganic nature. Similar TG profile was described by Lopes et al. [30]. In DEX + CSD mixture, only a slight anticipation of DEX decomposition was verified (T_{onset} = 247.82 °C) (Fig. 3b).

Lactose monohydrate (LAC) exhibited a typical TG profile of α-lactose isomer (Fig. 3c). Desorption of crystalline water was verified in the range of 139.00–151.23 °C with Δm = 5.23%, corresponding to the crystalline water content of α-lactose monohydrate [31, 32]. Thermal decomposition occurred in two major steps in the range of 225.76–319.33 °C (Δm = 59.51%) and gradually

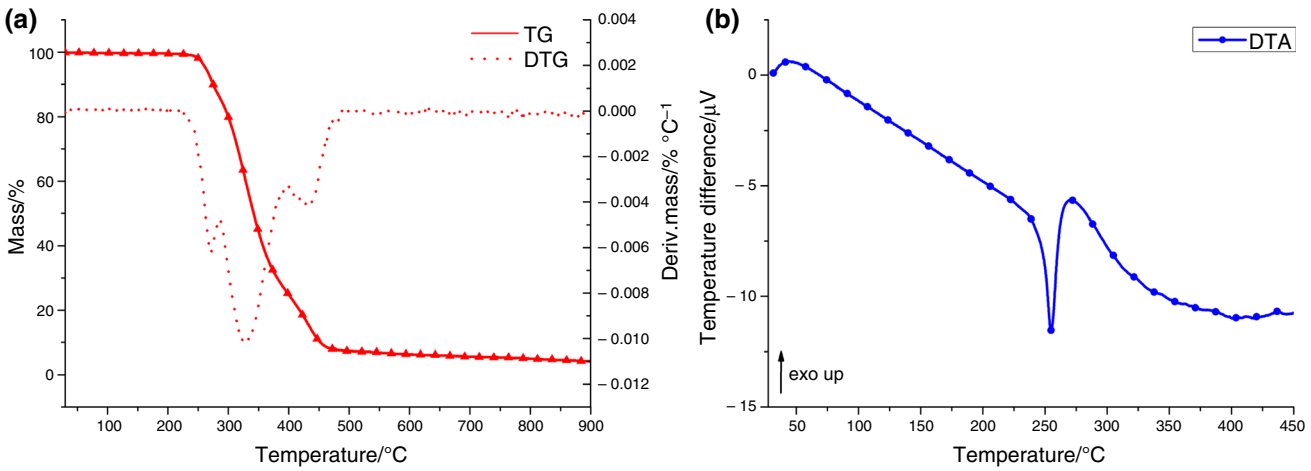

Fig. 2 TG/DTG (**a**) and DTA (**b**) curves of DEX

continued with increasing temperature. In DEX + LAC mixture, the decomposition process was slightly anticipated (T_{onset} = 227.50 °C).

The TG profile of mannitol (MAN) was characterized by a single-step decomposition event at 311.53–335.48 °C (Δm = 91.92%) (Fig. 3d). DEX thermal stability was increased in the binary mixture with this excipient. The decomposition process started at 266.67 °C—higher T_{onset} than that individually detected for DEX.

Microcrystalline cellulose 101 and 102 (MC101 and MC102, respectively) are excipients with the same chemical composition, but different particles size, and thus similar thermogravimetric profiles, were found for both compounds (Fig. 3e, f). Each curve showed mass loss events related to dehydration ($T_{peak/DTG}$ MC101 = 40.45 °C; $T_{peak/DTG}$ MC102 = 40.33 °C) and decomposition ($T_{peak/DTG}$ MC101 = 345.46 °C; $T_{peak/DTG}$ = 364.42 °C). TG profiles of both compounds are in agreement with that reported by Roumeli et al. [33]. DEX thermogravimetric profile was unaltered in the binary mixtures with both excipients, and therefore, no signs of interactions were found (Fig. 3e, f).

The TG profile of magnesium stearate (MS) was characterized by four mass loss events: The loss of superficial water was detected at 100.39–112.92 °C (Δm = 2.22%), followed by three decomposition steps in the range of 331.17–453.26 °C (Δm = 81.89%). In DEX + MS curve, a major decomposition step was detected in the range of 276.95–330.38 °C (Δm = 54.81%). Therefore, DEX thermal stability was not affected by the mixture with this excipient (Fig. 4a).

Polyvinylpyrrolidone K-30 (PVP) showed a dehydration event at 50.23–82.59 (Δm = 12.20%) followed by a single-step decomposition event in the range of 411.23–457.12 °C (Δm = 81.24%) (Fig. 4b). Decomposition of DEX + PVP mixture started at lower temperature (T_{onset} = 241.49 °C), indicating a slight decrease of DEX thermal stability.

Sodium starch glycolate (SSG) curve exhibited loss of surface water (44.99–74.33 °C; Δm = 10.49%) followed by a single-step decomposition event (265.56–306.46 °C, Δm = 49.03%). Decomposition of DEX + SSG mixture started at a lower temperature (T_{onset} = 231.13 °C) than that detected for each individual component (T_{onset} DEX = 256.60 °C; T_{onset} SSG = 265.56 °C) (Fig. 4c).

Corn starch (STA) showed two mass loss events: The first one (38.95–79.80 °C; Δm = 11.08%) is attributed to dehydration, and the second (302.59–326.68° C; Δm = 66.79%) is related to its decomposition [21]. DEX + STA mixture exhibited a single-step decomposition event in the range of 287.49–331.52 °C (Δm = 64.79%), followed by continuous mass loss with increasing temperature (Fig. 4d). Similar results were found for pre-gelatinized starch (PgSTA) and its binary mixture (Fig. 4e). Thus, DEX thermal stability was not affected in the mixtures with these excipients.

Talc (TAL) did not exhibit mass loss events within the studied temperature range (Fig. 4f). Due to its mineral nature ($Mg_3Si_4O_{10}(OH)_2$), thermal events only occur at temperatures above 800 °C [34]. In the binary mixture with this excipient, DEX decomposition was slightly anticipated (T_{onset} = 241.46 °C).

In general, DEX thermal stability was not abruptly affected in the binary mixtures with all excipients tested. Only slightly anticipations of the decomposition T_{onset} were observed and they are not enough to characterize API–excipient interactions. Hence, compatibility should be assessed using others analytical techniques.

Table 2 Thermogravimetric parameters of DEX, pharmaceutical excipients and its binary mixtures

Samples	Stage 1			Stage 2			Stage 3			Stage 4		
	T_{onset}–T_{endset}/°C	$T_{peak/DTG}$/°C	Δ*m*/%	T_{onset}–T_{endset}/°C	$T_{peak/DTG}$/°C	Δ*m*/%	T_{onset}–T_{endset}/°C	$T_{peak/DTG}$/°C	Δ*m*/%	T_{onset}–T_{endset}/°C	$T_{peak/DTG}$/°C	Δ*m*/%
DEX	256.60–276.73	267.25	12.49	303.85–359.12	327.34	57.56	410.32–454.49	438.54	18.95	–	–	–
CCS	38.27–79.22	53.51	12.52	282.34–309.35	296.45	38.82	436.50–446.17	443.31	3.64	–	–	–
DEX + CCS	47.95–59.86	48.77	5.51	246.11–260.50	255.29	8.19	288.51–340.50	320.25	51.77		–	
CSD	–	–	–	–	–	–	–	–	–	–	–	–
DEX + CSD	247.82–263.41	257.92	7.43	301.24–341.14	321.41	30.92	–	–	–	–	–	–
LAC	139.00–151.23	147.22	5.23	225.76–246.43	228.94	28.47	290.08–319.33	301.43	31.04	–	–	–
DEX + LAC	140.62–151.41	148.92	2.80	227.50–241.41	240.89	6.10	284.86–333.32	307.62	54.45	367.68–437.58	–	16.26
MAN	311.53–335.48	325.19	91.92	–	–	–	–	–	–	–	–	–
DEX + MAN	266.67–314.40	287.15	56.72	367.43–405.04	383.80	32.29	–	–	–	–	–	–
MC101	34.78–68.48	40.45	4.20	343.21–358.26	345.46	84.89	–	–	–	–	–	–
DEX + MC101	26.73–54.12	44.06	2.25	254.64–272.13	265.32	6.51	315.66–384.31	365.79	80.10	–	–	–
MC102	35.39–59.27	40.33	3.78	342.44–374.76	364.42	70.88	–	–	–	–	–	–
DEX + MC102	35.69–53.43	38.16	2.84	252.65–267.77	261.89	6.73	315.10–341.66	339.36	37.46	363.11–377.61	364.68	29.46
MS	100.39–112.92	107.28	2.22	331.17–339.44	350.58	23.13	431.34–453.26	437.00	8.78	–	–	–
DEX + MS	98.04–110.07	107.71	1.44	276.95–352.99	305.20	74.98	–	–	–	–	–	–
PVP	50.23–82.59	62.18	12.20	411.23–457.12	436.71	81.24	–	–	–	–	–	–
DEX + PVP	133.79–142.51	135.32	4.32	241.49–266.90	252.75	5.23	315.47–352.16	336.55	25.66	418.61–457.20	434.83	47.16
SSG	44.99–74.33	60.49	10.49	265.56–306.46	284.53	49.03	–	–	–	–	–	–
DEX + SSG	36.88–59.24	45.46	4.73	231.13–241.35	237.05	4.98	272.92–299.53	292.82	28.16	322.57–344.87	323.18	29.382
STA	38.95–79.80	60.94	11.08	302.59–326.68	315.46	66.79	–	–	–	–	–	–
DEX + STA	34.06–74.63	51.04	7.10	287.49–331.52	310.23	64.79	–	–		–	–	–
PgSTA	46.26–79.49	61.64	9.18	303.69–332.92	320.32	69.94	–	–	–	–	–	–
DEX + PgSTA	40.09–66.84	45.45	4.97	256.15–270.24	260.65	5.00	292.70–331.77	313.38	62.22	–	–	–
TAL	–	–	–	–	–	–	–	–	–	–	–	–
DEX + TAL	241.46–256.59	251.41	4.65	308.86–360.40	330.79	24.37	–	–	–	–	–	–

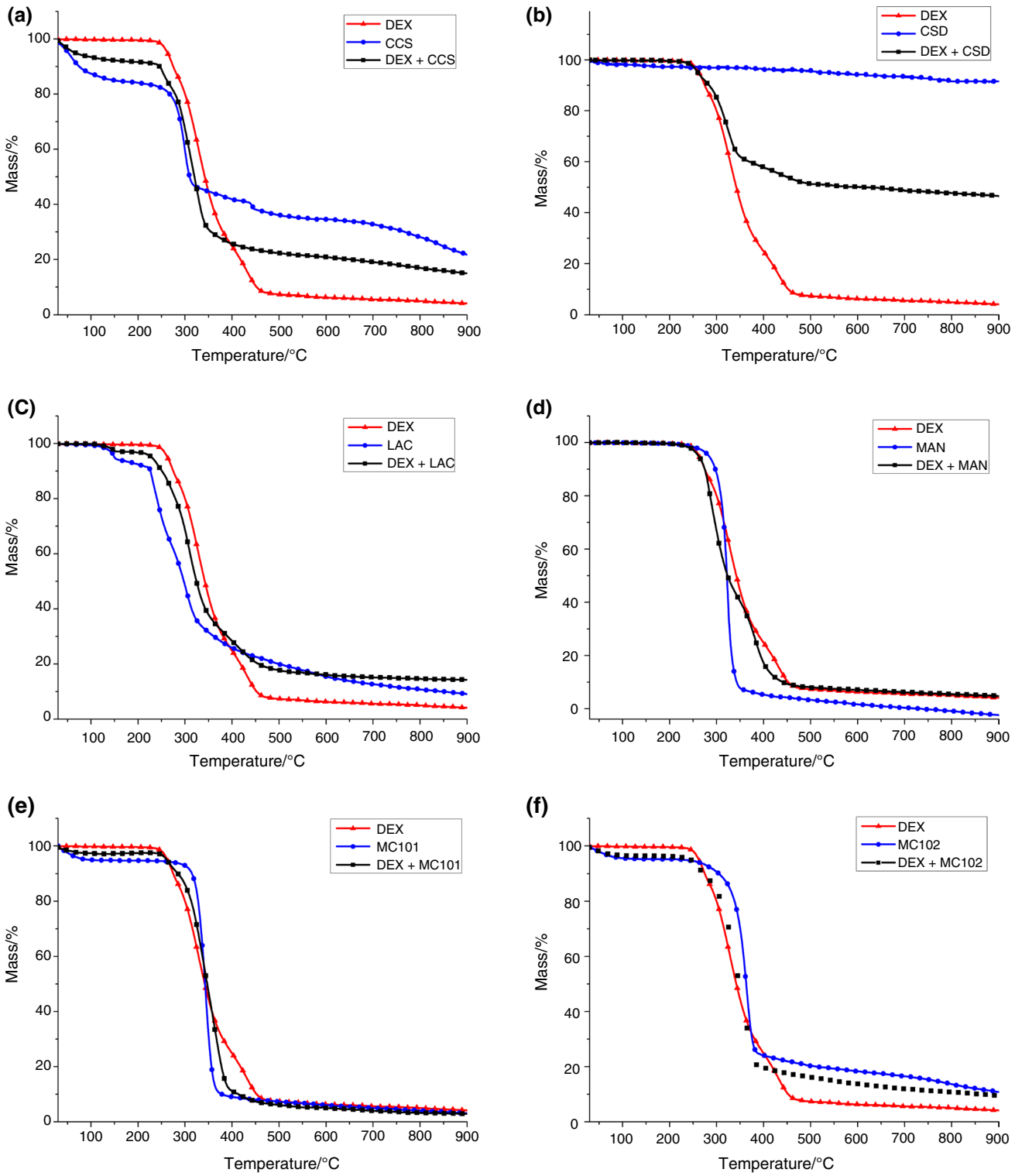

Fig. 3 TG curves of DEX binary mixtures with: **a** CCS, **b** CSD, **c** LAC, **d** MAN, **e** MC101 and **f** MC102

Thermal compatibility by DTA

The DTA parameters (T_{onset}, T_{endset}, T_{peak} and ΔH) of each individual component and its binary mixtures are shown in Table 3.

The DTA profile of CCS was characterized by three events: one endothermic ($T_{peak1} = 92.29$ °C) attributed to dehydration and two exothermic ($T_{peak2} = 296.58$ °C; $T_{peak3} = 317.39$ °C) related to sample decomposition. CCS

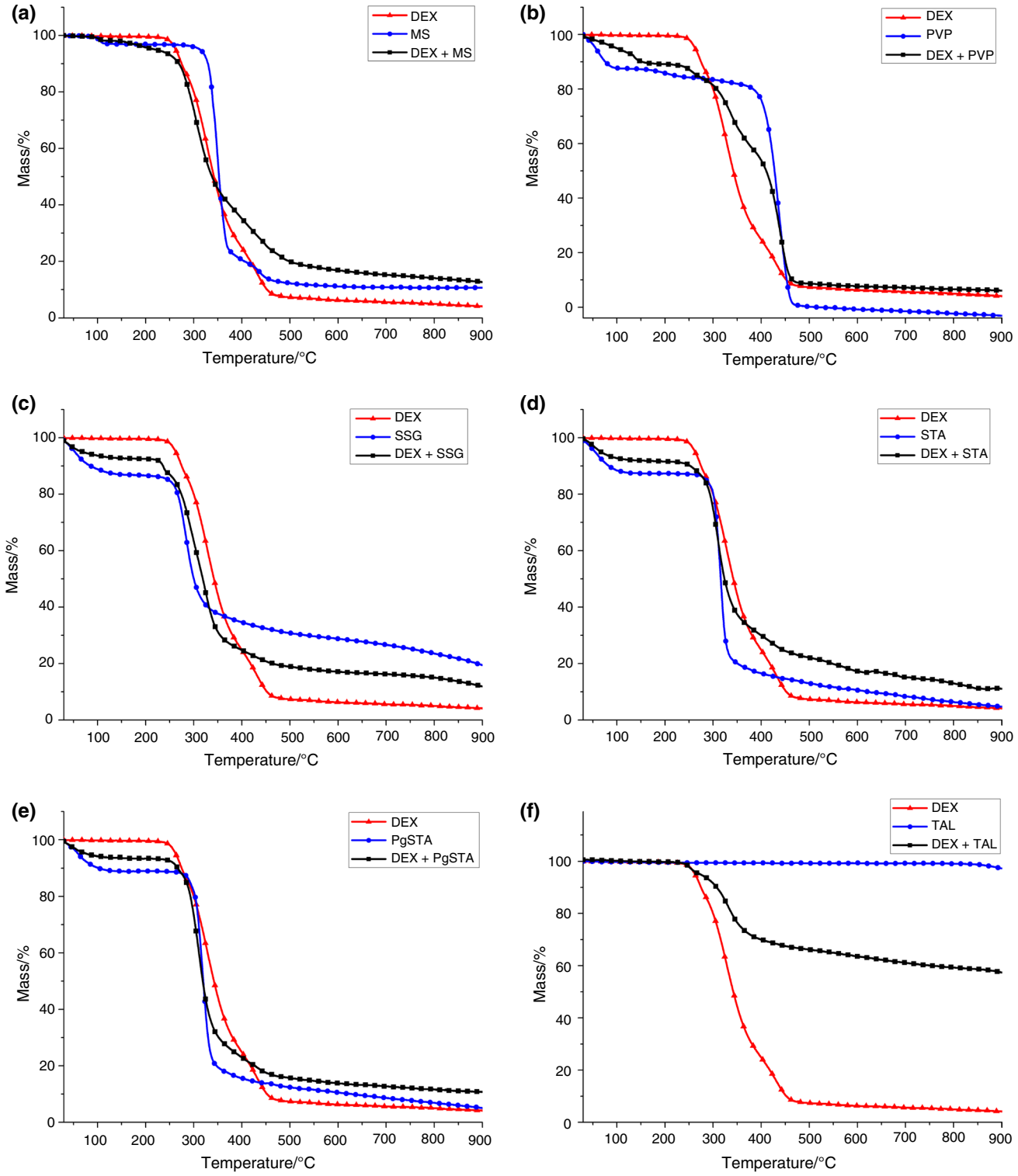

Fig. 4 TG curves of DEX binary mixtures with: **a** MS, **b** PVP, **c** SSG, **d** STA, **e** PgSTA and **f** TAL

thermal profile obtained in our research is in agreement with other studies reported in the literature [35, 36]. No evidence of interactions was found between DEX and CCS. In the DTA curve of the mixture, DEX melting peak was detected at 252.99 °C and the exothermic peak detected at 281.14 °C can be attributed to an overlapping of DEX and CCS decomposition peaks (Fig. 5a).

Table 3 DTA parameters of DEX, pharmaceutical excipients and its binary mixtures

Samples	Peak 1			Peak 2			Peak 3		
	T_{onset}–T_{endset}/°C	T_{peak}/°C	ΔH/J g^{-1}	T_{onset}–T_{endset}/°C	T_{peak}/°C	ΔH/J g^{-1}	T_{onset}–T_{endset}/°C	T_{peak}/°C	ΔH/J g^{-1}
DEX	248.76–260.27	254.86	− 388.79	262.59–296.50	270.48	–	–	–	–
CCS	47.58–125.28	92.29	− 509.16	272.83–308.68	296.58	91.96	313.41–327.08	317.39	18.79
DEX + CCS	65.19–110.30	94.39	− 225.33	243.40–262.47	252.99	–183.71	269.24–327.72	281.14	–
CSD	29.37–48.72	34.59	12.48	–	–	–	–	–	–
DEX + CSD	248.03–263.11	255.92	− 43.80	290.65–334.15	294.75	162.66	–	–	–
LAC	142.41–157.28	146.52	− 298.70	214.47–227.92	219.34	− 439.31	282.77–324.51	304.85	− 120.99
DEX + LAC	143.42–155.28	148.74	− 187.62	209.57–224.20	217.61	− 139.86	245.40–260.05	251.36	− 262.74
MAN	166.01–178.39	170.27	− 1.020.00	285.87–344.60	322.84	− 1.720.00	–	–	–
DEX + MAN	165.69–175.88	169.18	− 423.49	240.55–251.02	243.24	− 257.79	–	–	–
MC101	37.89–116.10	84.32	− 357.80	318.60–353.87	336.22	− 1310.00	–	–	–
DEX + MC101	245.12–265.24	259.20	− 116.47	285.33–320.44	308.57	− 229.27	–	–	–
MC102	36.85–109.29	76.57	− 340.35	330.08–376.62	360.54	− 870.71	–	–	–
DEX + MC102	251.84–268.04	262.85	− 43.05	279.53–320.03	307.45	− 136.87	–	–	–
MS	118.00–137.00	129.00	− 330.98	331.32–390.79	356.96	497.90	414.46–443.17	429.85	308.72
DEX + MS	119.57–136.30	127.93	− 220.66	265.62–291.36	274.91	77.17	–	–	–
PVP	37.50–125.04	97.61	− 750.84	408.04 –	431.40	–	–	–	–
DEX + PVP	87.23–129.99	109.35	− 233.05	266.08–307.04	286.83	318.07	–	–	–
SSG	46.30–127.66	92.01	− 589.69	274.47–298.55	283.28	146.94	317.62–350.24–	327.78	49.50
DEX + SSG	49.95–109.90	98.42	− 296.66	233.00–252.82	247.65	− 101.46	266.99–330.27	294.06	395.21
STA	40.72–140.97	88.36	− 733.54	287.30–327.19	315.33	− 300.98	–	–	–
DEX + STA	60.29–127.85	91.36	− 259.40	252.39–287.01	268.78	− 425.11	–	–	–
PgSTA	41.16–129.46	88.84	− 624.27	286.75–294.15	289.32	− 101.58	322.70–394.87	348.92	194.30
DEX + PgSTA	50.29–143.90	96.15	− 319.51	250.96–282.71	261.32	− 407.92	–	–	–
TAL	37.80–49.89	44.70	− 10.61	–	–	–	–	–	–
DEX + TAL	240.10–260.63	252.59	− 151.41	258.62–302.88	273.53	–	–	–	–

As already mentioned in TG results, no thermal events were detected for CSD due to its inorganic nature. The DTA curve of the binary mixture showed the DEX melting and decomposition peaks at 255.92 and 294.75 °C, respectively (Fig. 5b). However, there was an abrupt reduction in DEX melting enthalpy when compared to the individual curve. Although DEX + CSD mixture has been prepared in equal mass proportions (1:1), DC density is lower (0.029–0.042 g cm$^{3\ -1}$) than DEX (1.32 g cm$^{3\ -1}$), and consequently, its volume in the mixture was so much higher [23, 37]. It is possible that this volume difference has led to the detection of lower melting enthalpy for DEX in the binary mixture. Therefore, this result is not sufficient to characterize incompatibility between these compounds.

LAC exhibited a typical α-lactose DTA profile, as already verified in TG curve. The crystalline water desorption event was verified at 146.52 °C and the melting peak was detected at 219.34 °C. The third endothermic peak (T_{peak} = 304.85 °C) is related to sample decomposition, as also confirmed by TG curve. Thermal events from DEX and LAC were maintained in the DTA curve of their binary mixture, and thus no signs of interactions were found. The peaks corresponding to LAC crystalline dehydration and melting were detected at 148.74 °C and 217.61 °C, respectively, and DEX melting peak was detected at 251.36 °C (Fig. 5c).

MAN curve showed a melting peak at 170.27 °C and an endothermic peak attributed to sample decomposition at 322.84 °C. Similar thermal profiles for MAN have already been reported in the literature [21, 35]. In the binary mixture with this excipient (Fig. 5d), DEX melting peak was anticipated at approximately 12.00 °C (T_{peak} = 243.24 °C). Other authors have identified, using thermal analysis, interactions of MAN with atorvastatin, levodopa, nortriptyline, and omeprazole [38–41].

Similar DTA profiles were obtained for MC101 and MC102 (Fig. 5e, f, respectively). The first endothermic peak—detected at 84.32 °C for MC101 and at 76.57 °C for MC102—is characteristic of surface water loss. The second endothermic peak (T_{peak} MC101 = 336.22 °C; T_{peak} MC102 = 360.54 °C) is attributed to thermal decomposition, with higher enthalpy (ΔH) detected for MC101. Lavor et al. [42] and Lima et al. [35], using the DSC and DTA techniques, verified similar thermal profiles for MC101 and MC102, respectively. DEX thermal profile was affected

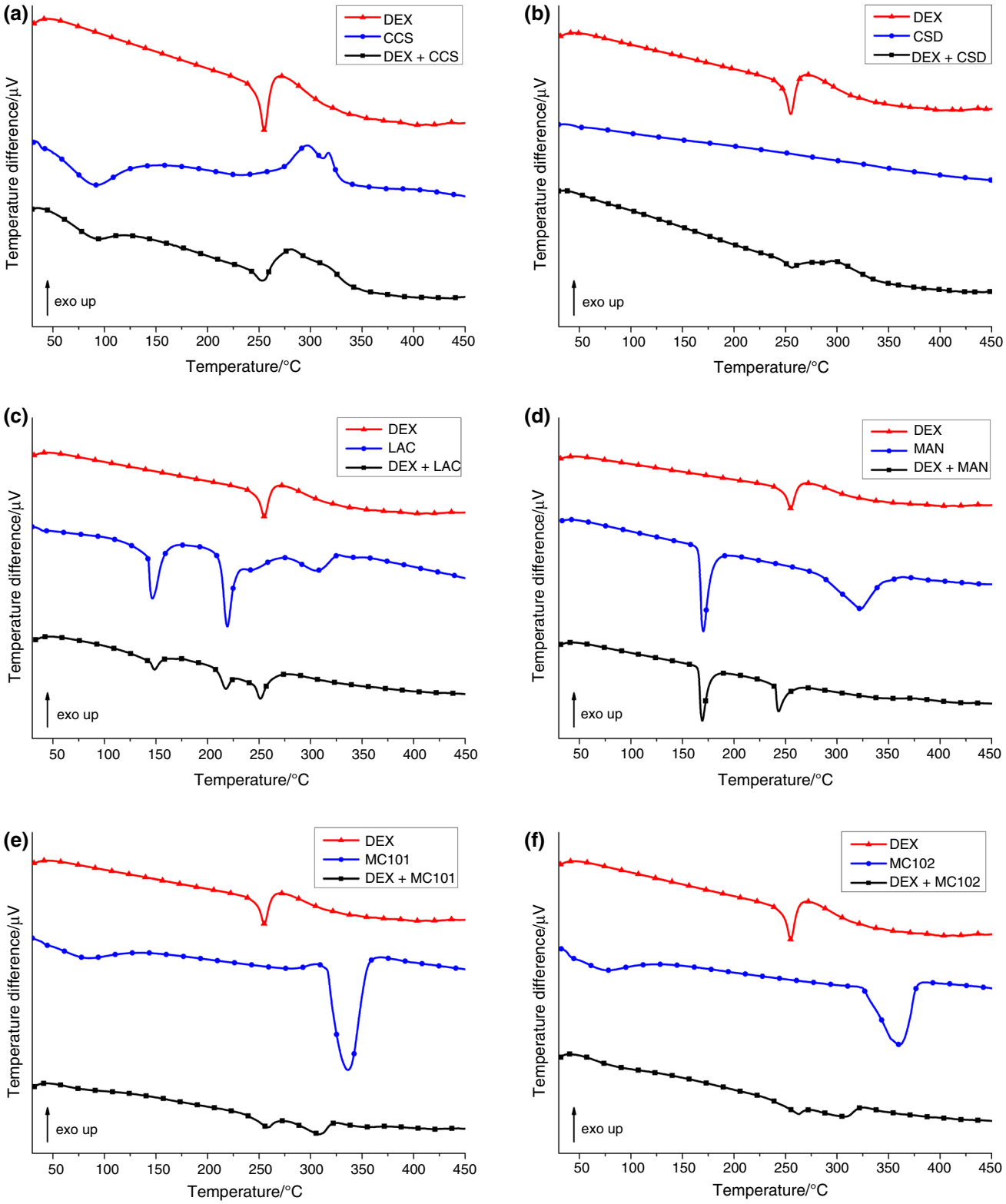

Fig. 5 DTA curves of DEX binary mixtures with: **a** CCS, **b** CSD, **c** LAC, **d** MAN, **e** MC101 and **f** MC102

by the mixture with both excipients. Briefly, DEX melting peaks were shifted to higher temperatures, which at first could indicate an improvement of thermal stability, but the melting enthalpy abruptly decreased in both mixtures. In addition, decomposition peaks of the excipients were anticipated to lower temperatures and also had abrupt enthalpy reduction.

MS first exhibited a melting peak at 129.00 °C, followed by a discrete endothermic peak possibly related to the melting of palmitate salt impurity [43]. At higher temperatures, two exothermic peaks attributed to sample decomposition were verified. This excipient induced the suppression of DEX melting peak, as shown in Fig. 6a. DTA curve of DEX + MS mixture only showed the melting peak of MS (T_{peak} = 127.93 °C) and a discrete exothermic peak (T_{peak} = 274.91 °C) at temperature near to DEX degradation. It is possible that the drug was dissolved in the previously molten excipient, assuming that both have certain miscibility. Another theory is that possible API–excipient interactions have altered the crystalline structure of DEX, making it more fragile and susceptible to fusion at lower temperatures [34]. In other studies, this excipient also induced the melting suppression of ibuprofen, meloxicam, tenofovir desoproxil fumarate, and diethylcarbamazine citrate [14, 44–46].

The DTA profile of PVP was characterized by two endothermic events: the first one is attributed to dehydration (T_{peak} = 97.61 °C) and the second is related to decomposition (T_{peak} = 431.40 °C), as confirmed by TG curve. This excipient induced the suppression of DEX melting peak, as shown in Fig. 6b. A possible explanation for this phenomenon is that the water emerged from PVP dehydration has induced the heat-facilitated dissolution of DEX [21]. Another theory is that DEX was dissolved in the elastic state of the polymer after its glass transition [47]. Other authors have reported thermal interactions of PVP with lipoic acid, diethylcarbamazine citrate and kaempferol [46, 48, 49].

SSG showed a melting peak at 91.01 °C and two exothermic peaks at 283.28 and 327.78 °C—both attributed to sample decomposition (Fig. 6c). Similar DTA curve for SSG was verified in Soares-Sobrinho et al. [50] study. In the binary mixture, DEX melting peak was slightly shifted to lower temperature (T_{peak} = 247.65 °C). However, small shifting or broadening of melting peaks do not characterize thermal incompatibility and can simply be attributed to the mixing process, which decreases the API purity in the binary mixture [51]. The exothermic peak detected at 294.06 °C is possibly an overlapping of DEX and SSG decomposition events.

Thermal profile of STA showed an endothermic peak characteristic of dehydration (T_{peak} = 88.36 °C) and another attributed to decomposition (T_{peak} = 315.33 °C). In the binary mixture, the endothermic peak detected at 268.78 °C is possibly an overlap of DEX melting peak and STA decomposition peak (Fig. 6d). Thus, DTA curves did not provide conclusive information about DEX + STA thermal compatibility. Similar results were obtained for PgSTA binary mixture (Fig. 6e).

No thermal events were verified for TAL, as previously described in the TG results. Furthermore, no evidence of interaction was found in DEX + TAL curve (Fig. 6f). The characteristic DEX melting and decomposition peaks were verified at 252.59 and 273.53 °C, respectively.

Compatibility study by FTIR

DEX FTIR spectra showed absorption bands characteristic of its chemical structure (Fig. 7). The broad band at 3390 cm^{-1} is attributed to the hydroxyl groups (O–H) stretching. The bands at 3000–2800 cm^{-1} are attributed to the stretching of C–H bonds of sp^3 carbon. Stretching vibrations of C-20 and C-3 carbonyl (C=O) groups were verified at 1707 and 1662 cm^{-1}, respectively. Absorption band at 1621 cm^{-1} is attributed to double bonds (C=C) conjugated to C-3 C=O group. Stretching and axial deformation bands from C–F bond were verified at 1269 and 893 cm^{-1}, respectively. Similar FTIR spectra for DEX were reported by Kumar et al. [52], Rodrigues et al. [53] and Silva et al. [54].

In DEX + CSD mixture, there was an overlapping of the Si–O stretching band from CSD (1250–1000 cm^{-1}), and consequently, it was not possible to assess some bands from DEX that absorbs in the same region (Fig. 7b). However, the overlapping of bands from inorganic compounds does not characterize API–excipient interactions in the binary mixture [41]. In addition, characteristic DEX absorption bands were maintained unchanged in other spectral regions.

Overlapping of excipient absorption bands was also verified in DEX + MS mixture at 3000–2810 cm^{-1} (C–H bonds stretching) and 1600–1450 cm^{-1} (COO^- stretching) regions (Fig. 8a). However, simple overlapping of bands is not conclusive evidence of API–excipient interactions.

Binary mixtures of DEX with CCS (Fig. 7a), LAC (Fig. 7c), MAN (Fig. 7d), MC101 (Fig. 7e), MC102 (Fig. 7f), PVP (Fig. 8b), SSG (Fig. 8c), STA (Fig. 8d), PgSTA (Fig. 8e) and TAL (Fig. 8f) showed no evidence of API–excipient interactions. In these binary mixtures, DEX infrared profile was maintained without changes like shifting, broadening, appearance or disappearance of vibrational bands.

Compatibility study by XRD

The XRD patterns of DEX, excipients and its binary mixtures are shown in Figs. 9 and 10. DEX diffractogram showed two intense peaks at 14.24 and 16.92° 2θ and secondary peaks at 7.56°, 10.72°, 12.60°, 13.72°, 15.18°, 15.70°, 17.80°, 18.58°, 22.84°, 23.56°, 26.78°, 28.02°,

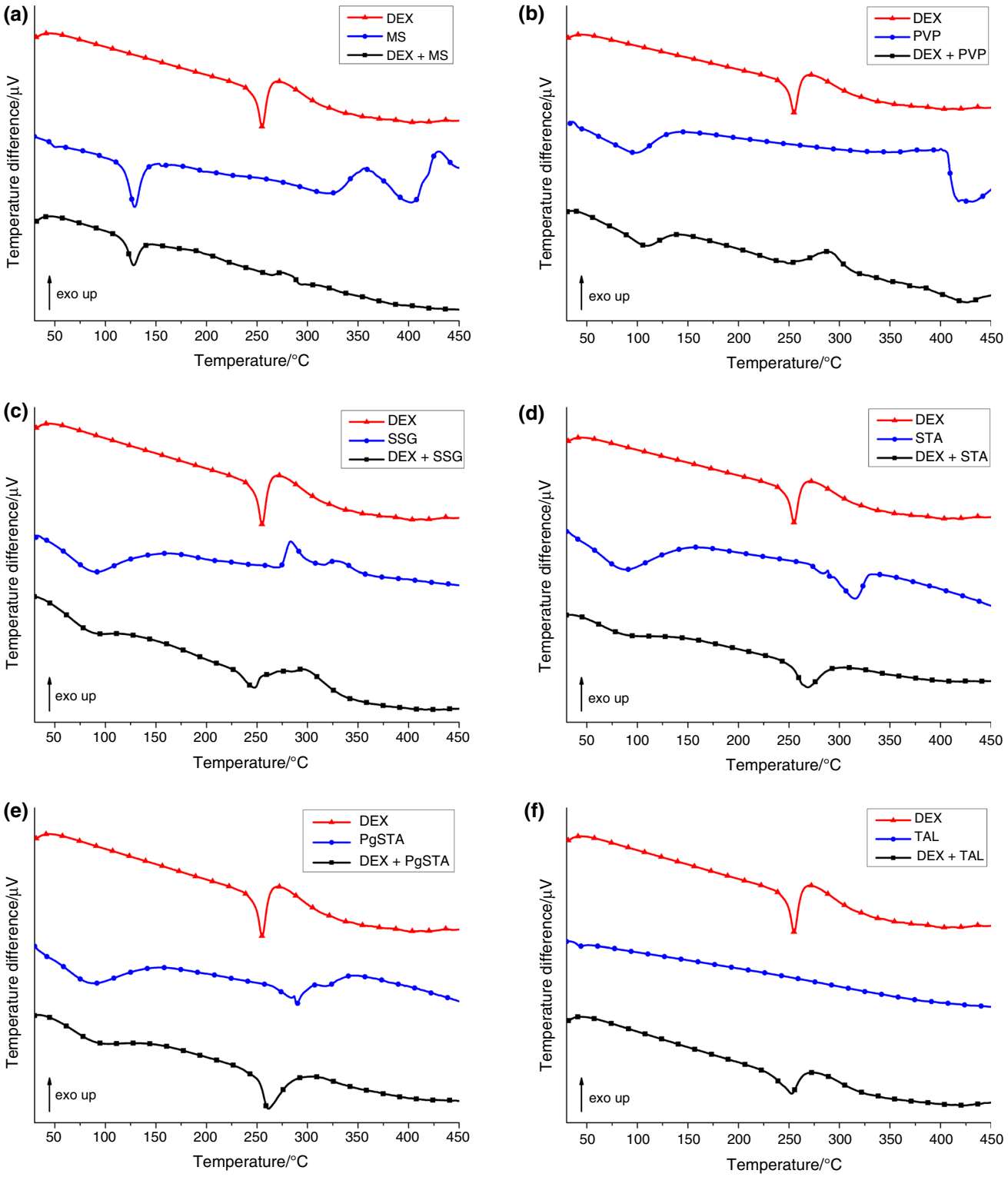

Fig. 6 DTA curves of DEX binary mixtures with: **a** MS, **b** PVP, **c** SSG, **d** STA, **e** PgSTA and **f** TAL

28.64°, and 30.20° 2θ. High-intensity sharp peaks followed by lower intensity peaks confirm the crystalline state of the sample [44]. The diffraction pattern obtained in our research is in agreement with the polymorphic form B of DEX reported by Oliveira et al. [29].

The main crystallinity peaks of DEX were identified in the diffractograms of all binary mixtures. Peaks intensity

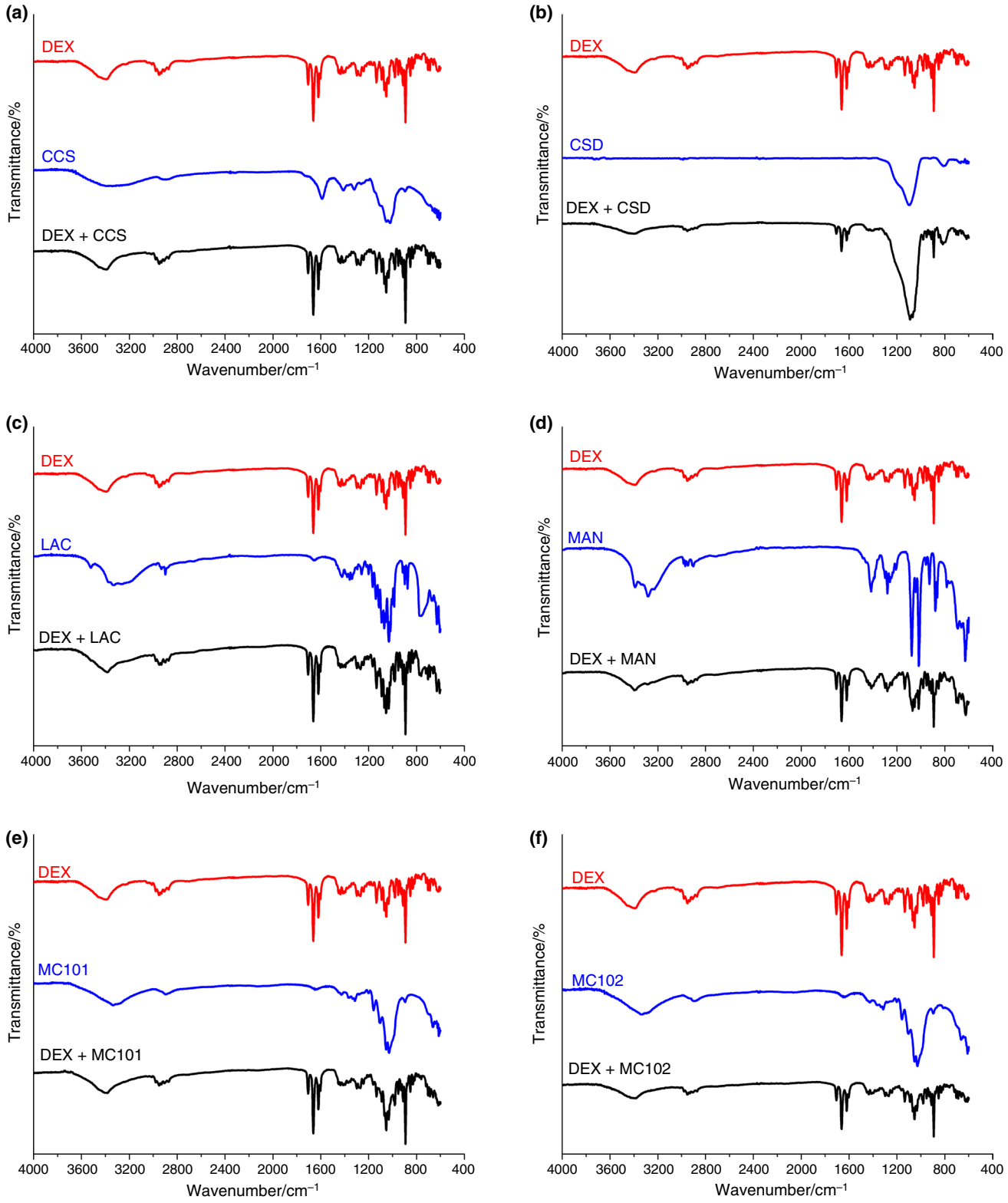

Fig. 7 FTIR spectra of DEX binary mixtures with: **a** CCS, **b** CSD, **c** LAC, **d** MAN, **e** MC101 and **f** MC102

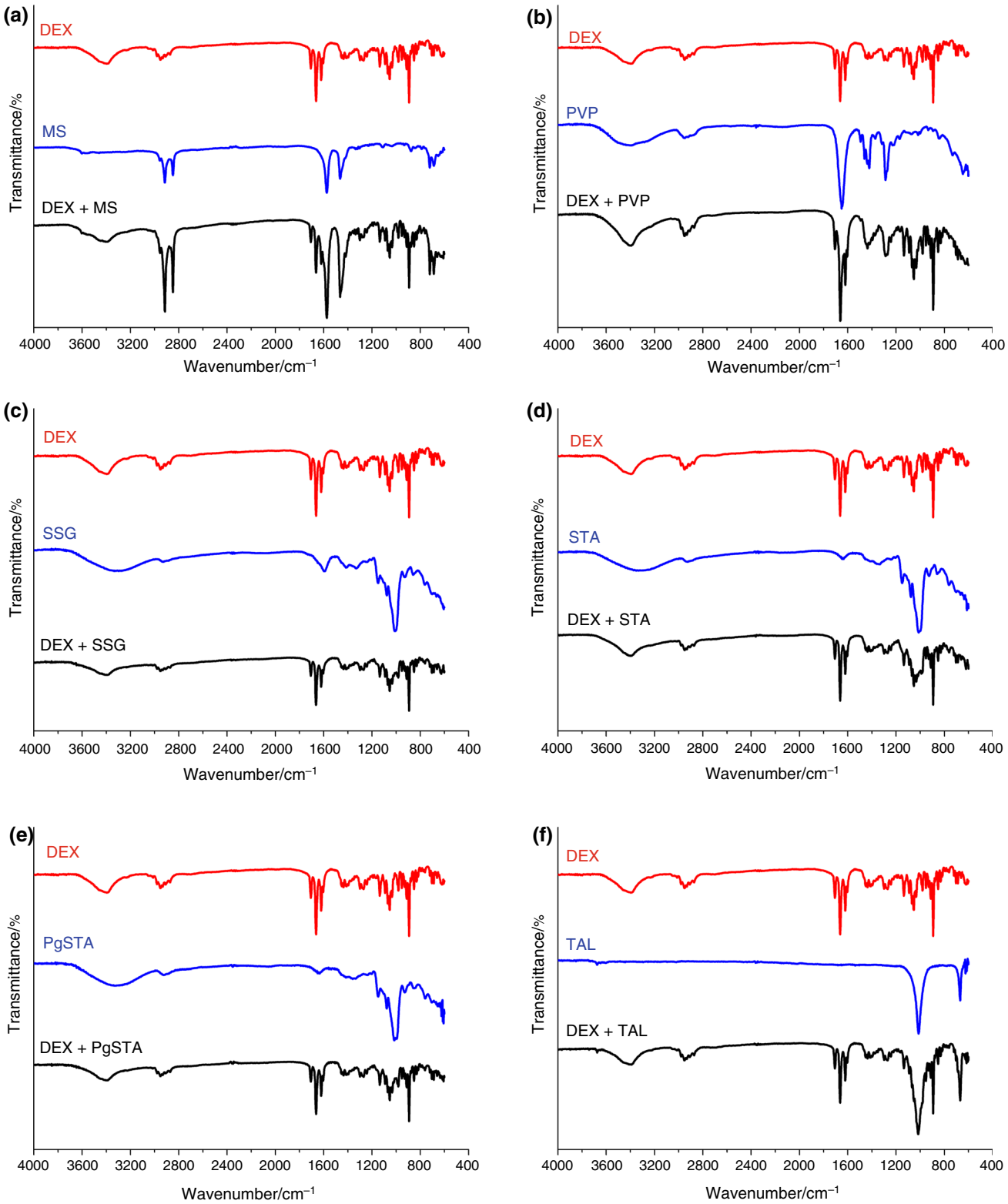

Fig. 8 FTIR spectra of DEX binary mixtures with: **a** MS, **b** PVP, **c** SSG, **d** STA, **e** PgSTA and **f** TAL

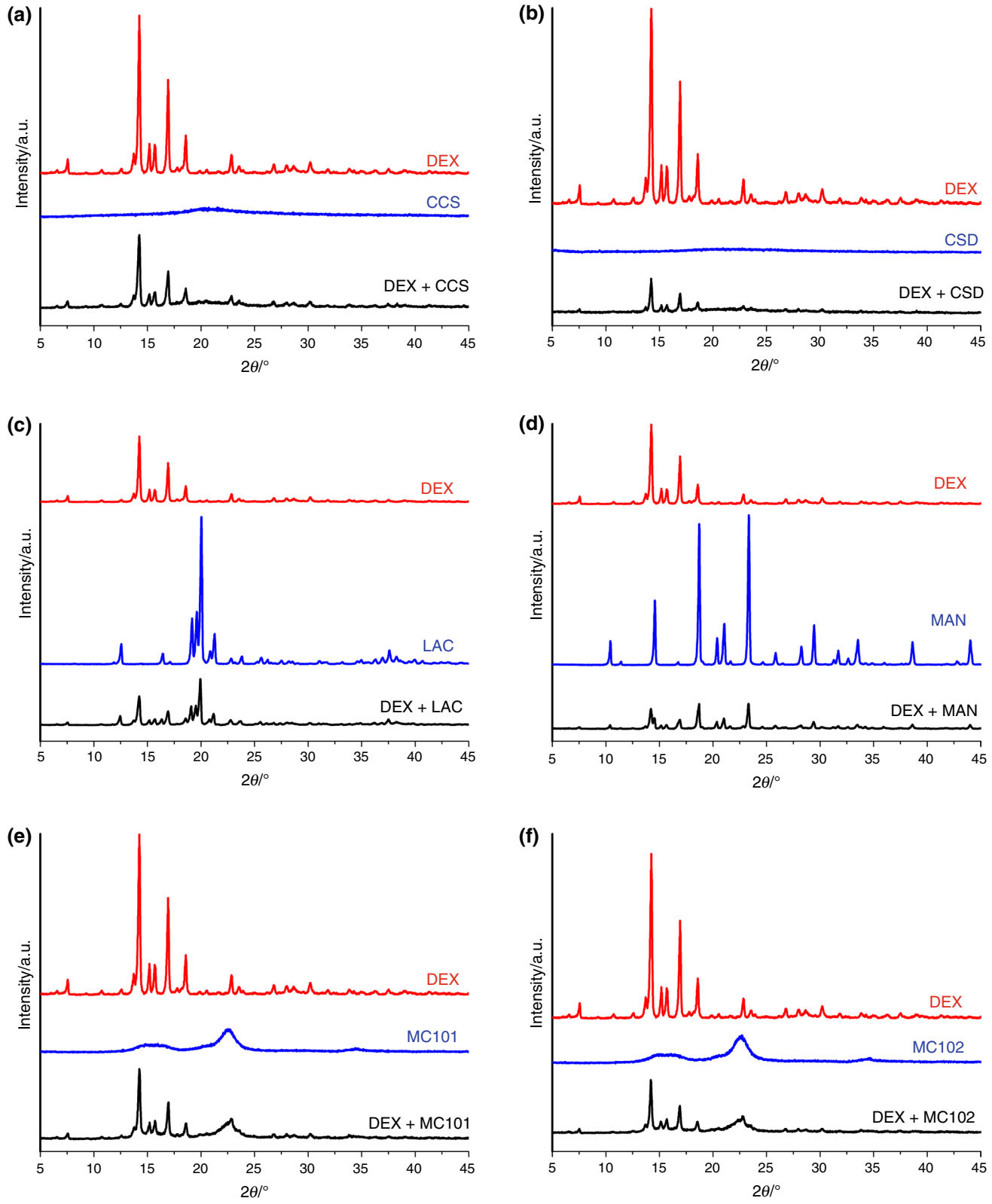

Fig. 9 XRD patterns of DEX binary mixtures with: **a** CCS, **b** CSD, **c** LAC, **d** MAN, **e** MC101 and **f** MC102

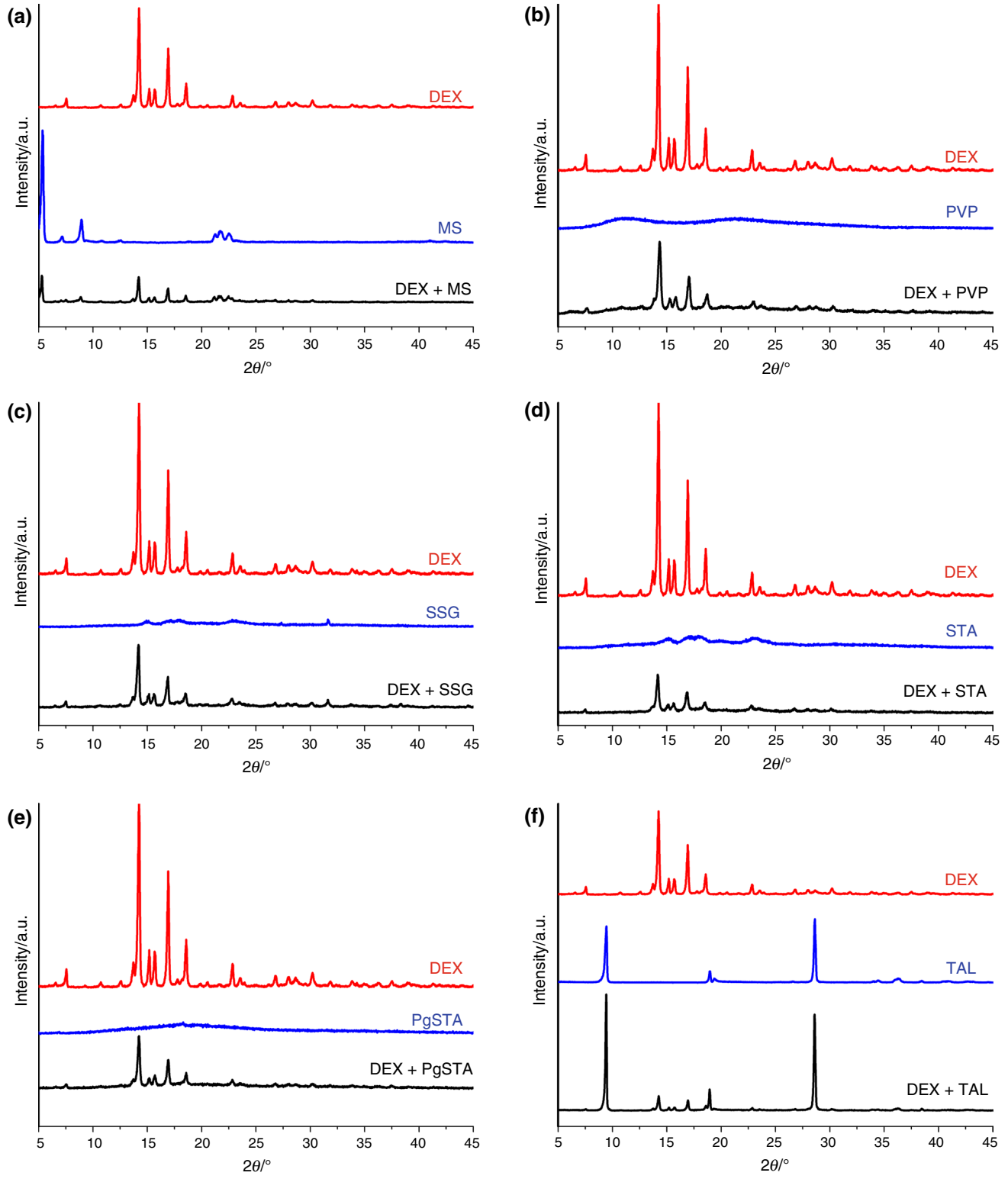

Fig. 10 XRD patterns of DEX binary mixtures with: **a** MS, **b** PVP, **c** SSG, **d** STA, **e** PgSTA and **f** TAL

decreased due to the lower API amount in the mixture (50%) when compared to the individual analysis (100%). Consequently, in most binary mixtures, low-intensity peaks were not identified. However, no interactions with modifications of DEX crystalline state were found.

Conclusions

Compatibility of dexamethasone with several solid excipients was assessed through different analytical techniques. Drug decomposition profile was not considerably affected by any excipient tested, as verified in TG curves. DTA technique pointed out alterations of drug melting temperature and/or enthalpy in the mixtures with mannitol, magnesium stearate, microcrystalline cellulose 101/102, and polyvinylpyrrolidone, which may characterize thermal interaction. FTIR and DRX were used as complementary techniques to confirm the interactions indicated by DTA and also to search for new interactions signs. Dexamethasone infrared absorption profile was not affected by the mixture with most tested excipients. FTIR spectra of magnesium stearate mixture did not provide conclusive information due to bands overlapping. X-ray diffractograms of all binary mixtures did not exhibit signs of interactions with changes of dexamethasone crystalline state. These results pointed that the interactions found by DTA technique were probably heat-induced. Therefore, the above-mentioned excipients should be carefully used in DEX solid dosage forms, especially in heat-based manufacturing processes as wet granulation. Further research should investigate the heat influence in these interactions.

Acknowledgements The authors acknowledge the fellowships received from Coordenação de Aperfeiçoamento de Pessoal de Nível Superior (CAPES) and Fundação de Apoio à Pesquisa do Estado da Paraíba (FAPESQ).

References

1. Bharate SS, Bharate SB, Bajaj AN. Interactions and incompatibilities of pharmaceutical excipients with active pharmaceutical ingredients: a comprehensive review. J Excip Food Chem. 2010;1:3–26.
2. ICH Harmonised Tripartite Guideline, Pharmaceutical Development: Q8(R2). In: International conference on harmonization of technical requirements for registrations of pharmaceutical for human use. Geneva: IFPMA; 2009.
3. Bandopadhyay S, Bandyopadhyay N, Deb PK, Singh C, Tekade RK. Preformulation studies of drug substances, protein, and peptides. In: Tekade RK, editor. Dosage form design considerations. Cambridge: Academic Press; 2018. p. 401–33. https://doi.org/10.1016/B978-0-12-814423-7.00012-5.
4. Yu LX, Amidon G, Khan MA, Hoag SW, Polli J, Raju GK, et al. Understanding pharmaceutical quality by design. AAPS J. 2014;16:771–83. https://doi.org/10.1208/s12248-014-9598-3.
5. Kurmi M, Sahu A, Ladumor MK, Kumar Bansal A, Singh S. Stability behaviour of antiretroviral drugs and their combinations. 9: identification of incompatible excipients. J Pharm Biomed Anal. 2019;166:174–82. https://doi.org/10.1016/j.jpba.2019.01.009.
6. Rojek B, Wesolowski M. FTIR and TG analyses coupled with factor analysis in a compatibility study of acetazolamide with excipients. Spectrochim Acta Part A Mol Biomol Spectrosc. 2019;208:285–93. https://doi.org/10.1016/j.saa.2018.10.020.
7. Chadha R, Bhandari S. Drug-excipient compatibility screening—role of thermoanalytical and spectroscopic techniques. J Pharm Biomed Anal. 2014;87:82–97. https://doi.org/10.1016/j.jpba.2013.06.016.
8. Narang AS, Desai D, Badawy S. Impact of excipient interactions on solid dosage form stability. Pharm Res. 2012;29:2660–83. https://doi.org/10.1007/s11095-012-0782-9.
9. Almeida L, Júnior JAO, Silva M, Nóbrega F, Andrade J, Santos W, et al. Tablet of *Ximenia americana* L. developed from mucoadhesive polymers for future use in oral treatment of fungal infections. Polymers. 2019;11:1–21. https://doi.org/10.3390/polym11020379.
10. Santana CP, Fernandes FHA, Brandão DO, Silva PCD, Correia LP, Nóbrega FP, Medeiros FD, Diniz PHGD, Véras G, Medeiros ACD. Compatibility study of dry extract of *Ximenia americana* L. and pharmaceutical excipients used in solid state. J Therm Anal Calorim. 2018;133:603–17. https://doi.org/10.1007/s10973-017-6764-8.
11. Fernandes FHA, Santana CP, Silva PCD, Simões MOS, Kaneko TM, Medeiros ACD. Development of a sunscreen by thermal compatibility study using *Schinopsis brasiliensis* Engler extract as preservative. J Therm Anal Calorim. 2018;131:753–63. https://doi.org/10.1007/s10973-017-6437-7.
12. Wanderley DMS, Melo DF, Silva LM, Silva WC, Correia LP, Oshiro-Junior JA, et al. Physical–chemical characterization of *N*-acylhydrazone derivative chitosan films using spectroscopic and thermoanalytical techniques. J Therm Anal Calorim. 2019;138:3789–96. https://doi.org/10.1007/s10973-019-08906-1.
13. Kacso I, Rus LM, Martin F, Miclaus M, Filip X, Dan M. Solid-state compatibility studies of Ketoconazole–Fumaric acid co-crystal with tablet excipients. J Therm Anal Calorim. 2020. https://doi.org/10.1007/s10973-020-09340-4.
14. da Silveira LM, Fiorot AB, Xavier TP, Yoshida MI, de Oliveira MA. Drug-excipient compatibility assessment of solid formulations containing meloxicam. Eur J Pharm Sci. 2018;112:146–51. https://doi.org/10.1016/j.ejps.2017.11.015.
15. Nie H, Mo H, Zhang M, Song Y, Fang K, Taylor LS, et al. Investigating the interaction pattern and structural elements of a drug–polymer complex at the molecular level. Mol Pharm. 2015;12:2459–68. https://doi.org/10.1021/acs.molpharmaceut.5b00162.
16. Fung MH, Devault M, Kuwata KT, Suryanarayanan R. Drug-excipient interactions: effect on molecular mobility and physical stability of ketoconazole–organic acid coamorphous systems. Mol Pharm. 2018;15:1052–61. https://doi.org/10.1021/acs.molpharmaceut.7b00932.
17. Ghaderi F, Nemati M, Siahi-Shadbad MR, Valizadeh H, Monajjemzadeh F. DSC kinetic study of the incompatibility of doxepin with dextrose: application to pharmaceutical preformulation studies. J Therm Anal Calorim. 2016;123:2081–90. https://doi.org/10.1007/s10973-015-4995-0.
18. Fuliaş A, Ledeţi I, Vlase G, Popoiu C, Hegheş A, Bilanin M, et al. Thermal behaviour of procaine and benzocaine. Part II: compatibility study with some pharmaceutical excipients used in solid dosage forms. Chem Cent J. 2013;7:140. https://doi.org/10.1186/1752-153X-7-140.
19. Rojek B, Wesolowski M. Compatibility studies of hydrocortisone with excipients using thermogravimetric analysis supported by multivariate statistical analysis. J Therm Anal Calorim. 2017;127:543–53. https://doi.org/10.1007/s10973-016-5441-7.
20. Rojek B, Wesolowski M. Compatibility study of theophylline with excipients using thermogravimetry supported by kinetic analysis.

J Therm Anal Calorim. 2020. https://doi.org/10.1007/s10973-019-09235-z.
21. Tita D, Jurca T, Fulias A, Marian E, Tita B. Compatibility study of the acetylsalicylic acid with different solid dosage forms excipients. J Therm Anal Calorim. 2013. https://doi.org/10.1007/s10973-013-2937-2.
22. Rojek B, Wesolowski M. Fourier transform infrared spectroscopy supported by multivariate statistics in compatibility study of atenolol with excipients. Vib Spectrosc. 2016;86:190–7. https://doi.org/10.1016/j.vibspec.2016.07.011.
23. U.S. National Library of Medicine. PubChem. 2020. https://pubchem.ncbi.nlm.nih.gov/compound/5743. Accessed 03 Mar 2020.
24. Keenan CR, Radojicic D, Li M, Radwan A, Stewart AG. Heterogeneity in mechanisms influencing glucocorticoid sensitivity: the need for a systems biology approach to treatment of glucocorticoid-resistant inflammation. Pharmacol Ther. 2015;150:81–93. https://doi.org/10.1016/j.pharmthera.2015.01.006.
25. Stahn C, Löwenberg M, Hommes DW, Buttgereit F. Molecular mechanisms of glucocorticoid action and selective glucocorticoid receptor agonists. Mol Cell Endocrinol. 2007;275:71–8. https://doi.org/10.1016/j.mce.2007.05.019.
26. Canadian Institutes of Health Research, Alberta Innovates—Health Solution, The Metabolomics Innovation Centre (TMIC). Drugbank. 2020. https://www.drugbank.ca/drugs/DB01234. Accessed 03 Mar 2020.
27. Agência Nacional de Vigilância Sanitária. Dexamethasone—Offical Monograph IF55-00. In: Farmacopeia Brasileira. Brasília: Agência Nacional de Vigilância Sanitária; 2019. pp. 702–4.
28. The Ministry of Health, Labour and Welfare. Dexamethasone—Official Monograph. In: Japanese pharmacopoeia. Tokyo: The Ministry of Health, Labour and Welfare; 2016. pp. 699–700.
29. Oliveira PFM, Willart J-F, Siepmann J, Siepmann F, Descamps M. Using milling to explore physical states: the amorphous and polymorphic forms of dexamethasone. Cryst Growth Des. 2018;18:1748–57. https://doi.org/10.1021/acs.cgd.7b01664.
30. Lopes MS, Catelani TA, Nascimento ALCS, Garcia JS, Trevisan MG. Ketoconazole: compatibility with pharmaceutical excipients using DSC and TG techniques. J Therm Anal Calorim. 2019. https://doi.org/10.1007/s10973-019-09137-0.
31. Smith G, Hussain A, Bukhari NI, Ermolina I. Quantification of residual crystallinity in ball milled commercially sourced lactose monohydrate by thermo-analytical techniques and terahertz spectroscopy. Eur J Pharm Biopharm. 2015;92:180–91. https://doi.org/10.1016/j.ejpb.2015.02.026.
32. Badal Tejedor M, Pazesh S, Nordgren N, Schuleit M, Rutland MW, Alderborn G, et al. Milling induced amorphisation and recrystallization of α-lactose monohydrate. Int J Pharm. 2018;537:140–7. https://doi.org/10.1016/j.ijpharm.2017.12.021.
33. Roumeli E, Tsiapranta A, Pavlidou E, Vourlias G, Kachrimanis K, Bikiaris D, et al. Compatibility study between trandolapril and natural excipients used in solid dosage forms. J Therm Anal Calorim. 2013;111:2109–15. https://doi.org/10.1007/s10973-012-2476-2.
34. Liu X, Liu X, Hu Y. Investigation of the thermal decomposition of talc. Clays Clay Miner. 2014;62:137–44. https://doi.org/10.1346/CCMN.2014.0620206.
35. Lima NGPB, Lima IPB, Barros DMC, Oliveira TS, Raffin FN, De Lima E Moura TFA, et al. Compatibility studies of trioxsalen with excipients by DSC, DTA, and FTIR. J Therm Anal Calorim. 2014. https://doi.org/10.1007/s10973-013-3216-y.
36. Pereira MAV, Fonseca GD, Silva-Júnior AA, Fernandes-Pedrosa MF, De M, Barbosa EG, et al. Compatibility study between chitosan and pharmaceutical excipients used in solid dosage forms. J Therm Anal Calorim. 2014. https://doi.org/10.1007/s10973-014-3769-4.
37. Rowe R, Sheskey P, Quinn M. Handbook of pharmaceutical excipients. 6th ed. London, Washington: Pharmaceutical Press and American Pharmacists Association; 2009.
38. Da Silva EP, Pereira MAV, De Barros Lima IP, Lima NGPB, Barbosa EG, Aragão CFS, et al. Compatibility study between atorvastatin and excipients using DSC and FTIR. J Therm Anal Calorim. 2016;123:933–9. https://doi.org/10.1007/s10973-015-5077-z.
39. Ledeti I, Bolintineanu S, Vlase G, Circioban D, Ledeti A, Vlase T, et al. Compatibility study between antiparkinsonian drug Levodopa and excipients by FTIR spectroscopy, X-ray diffraction and thermal analysis. J Therm Anal Calorim. 2017;130:433–41. https://doi.org/10.1007/s10973-017-6393-2.
40. Ledeţi I, Budiul M, Matusz P, Vlase G, Circioban D, Dehelean C, et al. Preformulation studies for nortriptyline: solid-state compatibility with pharmaceutical excipients. J Therm Anal Calorim. 2018;131:191–9. https://doi.org/10.1007/s10973-017-6269-5.
41. Agatonovic-Kustrin S, Markovic N, Ginic-Markovic M, Mangan M, Glass BD. Compatibility studies between mannitol and omeprazole sodium isomers. J Pharm Biomed Anal. 2008;48:356–60. https://doi.org/10.1016/j.jpba.2008.02.009.
42. Lavor EP, Navarro MVM, Freire FD, Aragão CFS, Raffin FN, Barbosa EG, et al. Application of thermal analysis to the study of antituberculosis drugs-excipient compatibility. J Therm Anal Calorim. 2014;115:2303–9. https://doi.org/10.1007/s10973-013-3050-2.
43. Shantikumar S, Sreekanth G, Surendranath KV, Jafervalli S, Satheeshkumar N. Compatibility study between sitagliptin and pharmaceutical excipients used in solid dosage forms. J Therm Anal Calorim. 2014;115:2423–8. https://doi.org/10.1007/s10973-013-3329-3.
44. Silva JPA, Figueirêdo CBM, de Medeiros Vieira ACQ, de Lyra MAM, Rolim LA, Rolim-Neto PJ, et al. Thermal characterization and kinetic study of the antiretroviral tenofovir disoproxil fumarate. J Therm Anal Calorim. 2017;130:1643–51. https://doi.org/10.1007/s10973-017-6477-z.
45. Tiţa B, Fuliaş A, Szabadai Z, Rusu G, Bandur G, Tiţa D. Compatibility study between ibuprofen and excipients in their physical mixtures. J Therm Anal Calorim. 2011;105:517–27. https://doi.org/10.1007/s10973-010-1188-8.
46. Chaves LL, Rolim LA, Gonçalves MLCM, Vieira ACC, Alves LDS, Soares MFR, et al. Study of stability and drug-excipient compatibility of diethylcarbamazine citrate. J Therm Anal Calorim. 2013;111:2179–86. https://doi.org/10.1007/s10973-012-2775-7.
47. de Souza CMP, dos Santos JAB, do Nascimento AL, Chaves Júnior JV, de Lima Ramos Júnior FJ, de Lima Neto SA, et al. Thermal analysis study of solid dispersions hydrochlorothiazide. J Therm Anal Calorim. 2018;131:681–9. https://doi.org/10.1007/s10973-017-6091-0.
48. Silva PCD, Portela AS, Lima RSC, Santana CP, Medeiros ACD, Da Silva Simões MO. Compatibility study between lipoic acid with polymers used in controlled drug release systems. J Therm Anal Calorim. 2016;123:965–71. https://doi.org/10.1007/s10973-015-4850-3.
49. de Lima Melchiades G, Angeli VW, Colombo M, Koester LS. Investigation of the compatibility between kaempferol and excipients by thermal, spectroscopic and chemometric methods. J Therm Anal Calorim. 2019. https://doi.org/10.1007/s10973-019-09092-w.
50. Soares-Sobrinho JL, De La Roca Soares MF, Lopes PQ, Correia LP, De Souza FS, Macêdo RO, et al. A preformulation study of a new medicine for chagas disease treatment: physicochemical characterization, thermal stability, and compatibility of benznidazole. AAPS PharmSciTech. 2010;11:1391–6. https://doi.org/10.1208/s12249-010-9495-8.

51. Tita B, Ledeti I, Bandur G, Tita D. Compatibility study between indomethacin and excipients in their physical mixtures. J Therm Anal Calorim. 2014;118:1293–304. https://doi.org/10.1007/s10973-014-3986-x.
52. Kumar V, Leekha A, Tyagi A, Kaul A, Mishra AK, Verma AK. Preparation and evaluation of biopolymeric nanoparticles as drug delivery system in effective treatment of rheumatoid arthritis. Pharm Res. 2017;34:654–67. https://doi.org/10.1007/s11095-016-2094-y.
53. Rodrigues LB, Leite HF, Yoshida MI, Saliba JB, Junior ASC, Faraco AAG. In vitro release and characterization of chitosan films as dexamethasone carrier. Int J Pharm. 2009;368:1–6. https://doi.org/10.1016/j.ijpharm.2008.09.047.
54. Da Silva GR, Da Silva-Cunha A, Behar-Cohen F, Ayres E, Oréfice RL. Biodegradable polyurethane nanocomposites containing dexamethasone for ocular route. Mater Sci Eng C. 2011;31:414–22. https://doi.org/10.1016/j.msec.2010.10.019.